Some gravitational aspects of scalar field dark matter

Patrick Valageas

IPhT - CEA Saclay

Collaboration with Ph. Brax, A. Boudon, R. Galazo-Garcia, J. Cembranos, C. Burrage, L. K. Wong

ADE/CoPhy, January 29, 2026

Dark Matter

I- Evidence

II- Ultra-Light Dark Matter

III- Scalar-Field Dark Matter models (SFDM)

IV- Quartic self-interaction

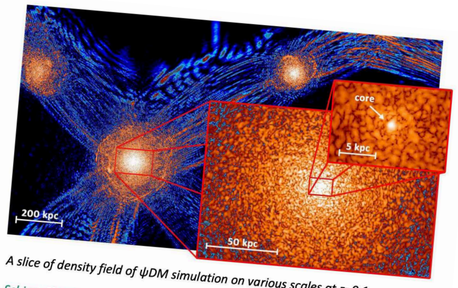

A slice of density field of ψDM simulation on various scales at z=0.1

Schive, Chiueh, and Broadhurst (2014)

Galaxy-scale dynamics: Formation of SFDM halos with a flat core

I- Non-relativistic regime

II- Soliton

III- Soliton formation

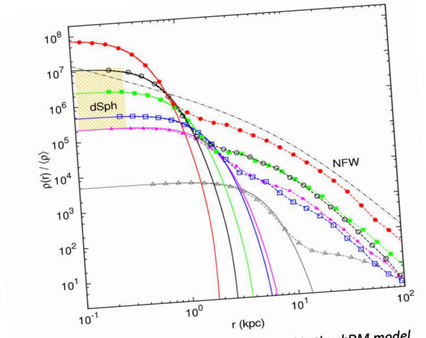

Radial density profiles of haloes formed in the ψDM model

Vortex lines and rotating soliton

I- Vortices

II- Many vortices

III- Continuum limit

IV- Numerical simulations

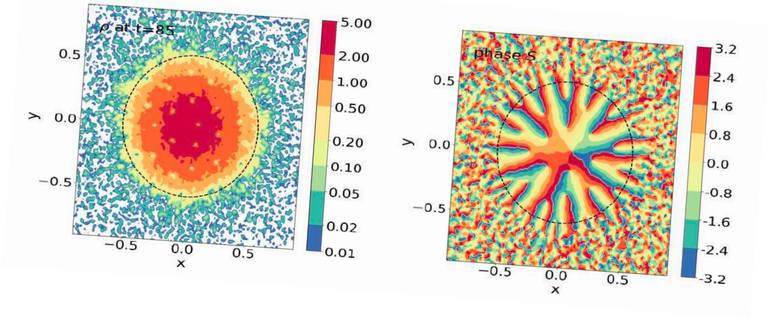

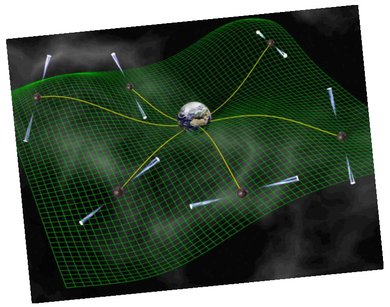

Detecting scalar dark matter clumps with pulsar timing arrays

I- Radial infall onto a BH

II- BH moving inside a SFDM cloud (soliton)

III- Subsonic regime

IV- Supersonic regime

I- DARK MATTER

Rich evidence for Dark Matter through its gravitational effects, from galactic to cosmological scales.

- 1933, Zwicky: motion of galaxies in the Coma cluster
- 1970s, Bosma, Rubin: rotation curves of spiral galaxies
- 1970s, Ostriker, Peebles: stability of disks in spiral galaxies
- 1980s, Peebles, Primack, Bond, White, …: Cosmic Microwave Background, Gravitational lensing, mass in X-ray clusters, …

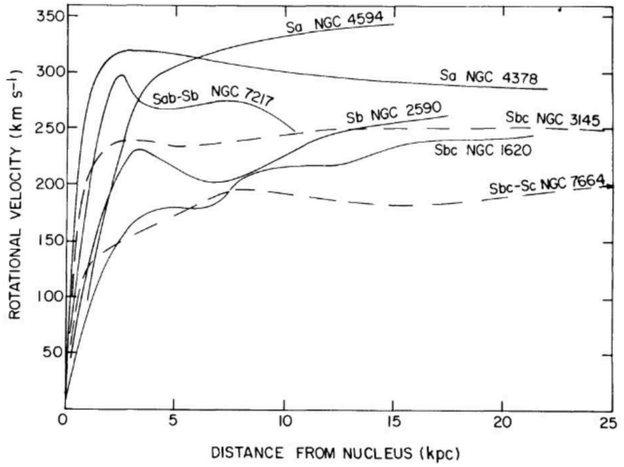

Rotational velocities for seven galaxies as a function of distance from nucleus.
Rubin et al. (1978).

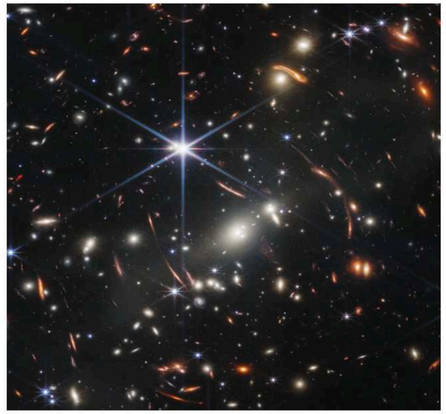

Gravitational lensing in Webb's First Deep Field taken by JWST (2022).
Galaxy cluster SMACS 0723
Credit edit: NASA, ESA, CSA, and STScI

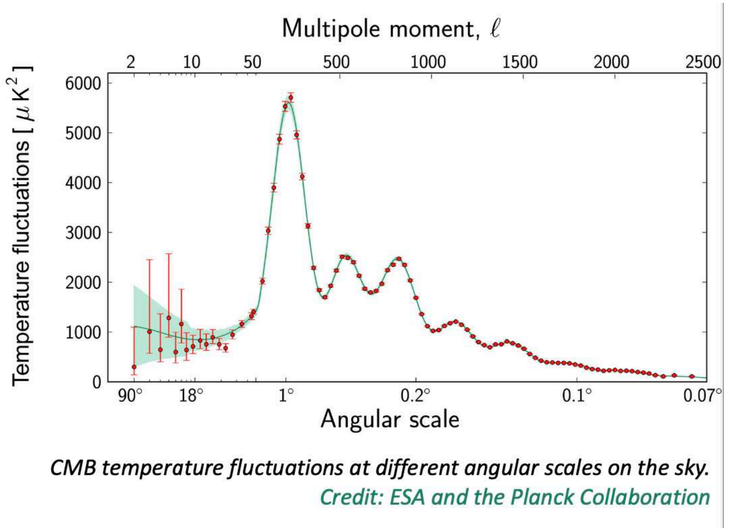

CMB temperature fluctuations at different angular scales on the sky.
Credit: ESA and the Planck Collaboration

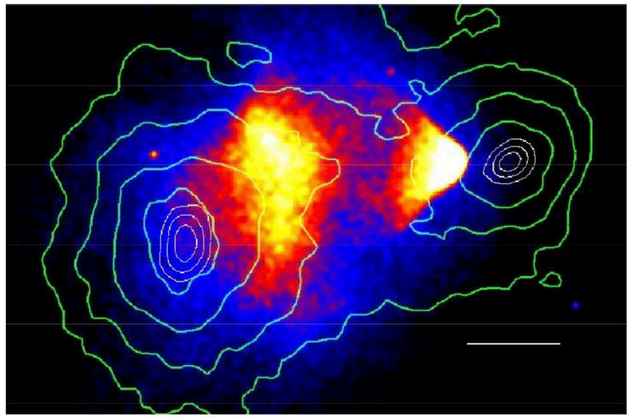

Bullet cluster (Clown et al. 2006): colors=X-ray gas, green isocontours=projected density measured by gravitational lensing

A- Known properties of DM

- 27% of the energy density of the universe
- Cold (non-relativistic)
- Dark: small electromagnetic interactions
- Collisionless / pressureless: small self-interactions or interactions with baryons

Energy content of the Universe

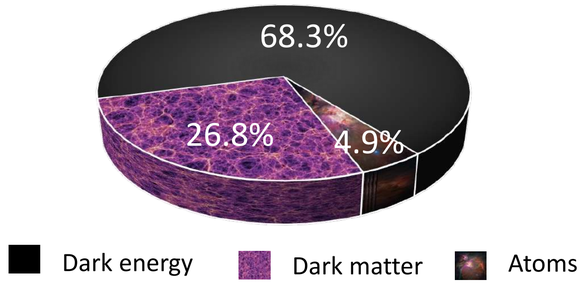

However there remains a huge uncertainty on its mass and many scenarios exist, from elementary particles to macroscopic objects:

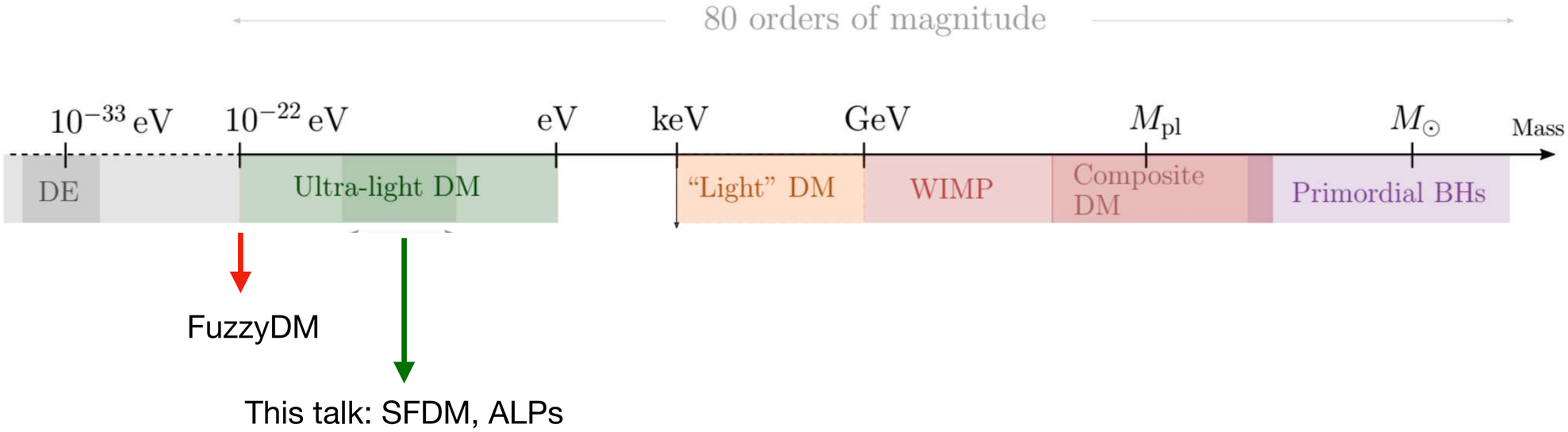

B- Many DM candidates

Bertone and Tait, 1810.01668

II- Ultra-Light Dark Matter

Renewed interest in recent years (Hui, Ostriker, Tremaine, Witten 2017), especially since WIMPs have not been detected yet and ULDM might alleviate some small-scale tensions of LCDM.

Missing satellite problem

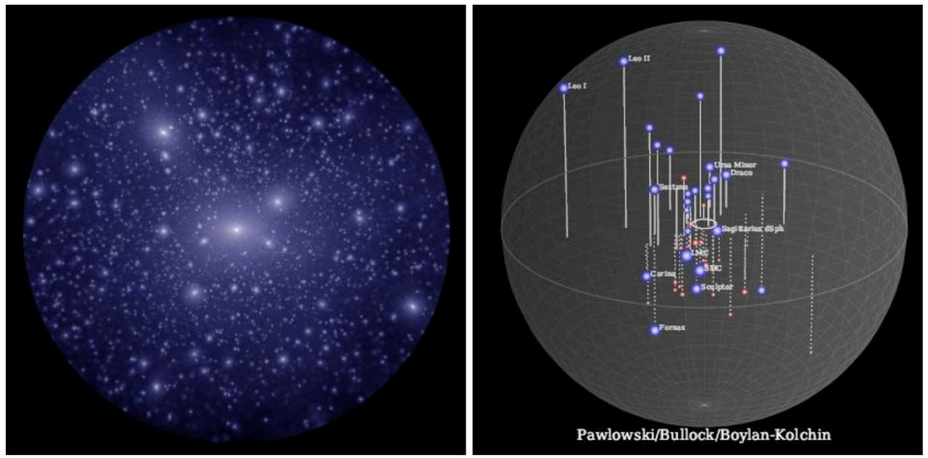

Predicted ΛCDM substructure

Simulation by V. Robles and T. Kelley and collaborators.

Known Milky Way satellites

James S. Bullock, M. Boylan-Kolchin, M. Pawlowski

Core/cusp problem

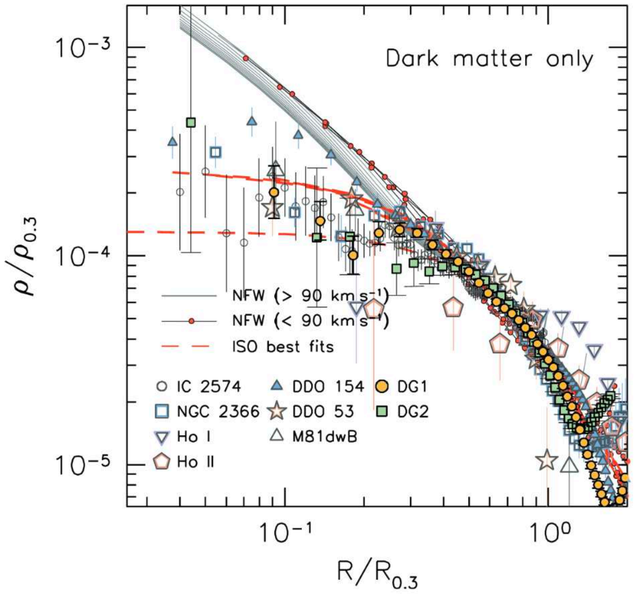

Density profiles observations and simulations

Antonino Popolo, Morgan Le Delliou (2017)

These problems may be solved by a proper account of baryonic physics (feedback from Supernovae and AGN), but ULDM remains an interesting candidate on its own.

A- Fuzzy Dark Matter

De Broglie wavelength: $$\lambda_{\rm dB} = 2\pi/(mv) \simeq \left(\frac{m}{10^{-22}\,{\rm eV}}\right)^{-1}\left(\frac{v}{100\,{\rm km/s}}\right)^{-1}{\rm kpc}$$

→ The DM density field behaves like CDM on large scales but structures are suppressed below $\lambda_{\rm dB}$

In particular, hydrostatic flat cores (« solitons ») can form at the center of DM halos.

For Fuzzy Dark Matter: $m \sim 10^{-22}{\rm eV}$ $\lambda_{\rm dB} \sim 1\,{\rm kpc}$

However, this model already seems ruled out by Lyman-alpha forest power spectra (because of this suppression of small-scale power).

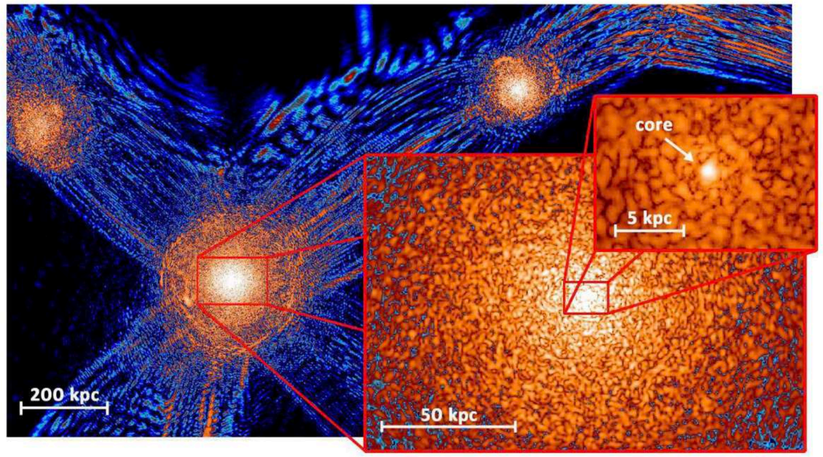

A slice of density field of ψDM simulation on various scales at z=0.1

Schive, Chiueh, and Broadhurst (2014)

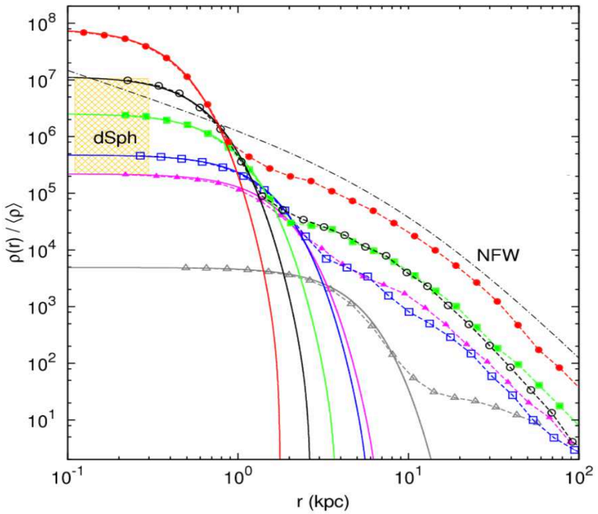

Radial density profiles of haloes formed in the ψDM model

In the FDM model, the wavelike dynamics below λ_{dB} , which leads to the suppression of small-scale power, appears as an effective « quantum pressure » in the hydrodynamical regime.

B- Scalar field Dark Matter with self-interactions

Instead of relying on this quantum pressure (large λ_{dB}), we can also suppress small-scale structures through self-interactions.

This also generates an effective pressure, which is now due to the self-interactions.

III- Scalar-field models

$$S_\phi = \int d^4x\sqrt{-g}\left[-\frac{1}{2}g^{\mu\nu}\partial_\mu\phi\partial_\nu\phi - V(\phi)\right].$$

Background:

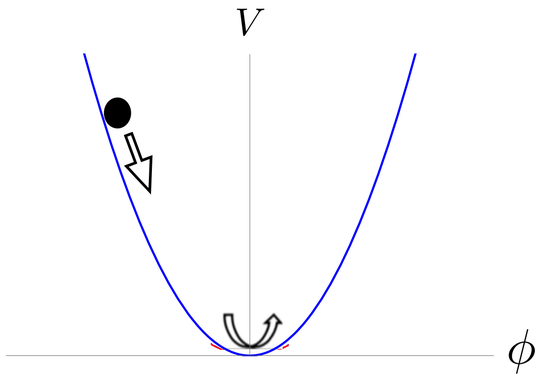

Klein-Gordon . eq.: $\ddot{\phi} + 3H\dot{\phi} + \frac{dV}{d\phi} = 0$

e.g., no self-interactions: $V = \frac{1}{2}m^2\phi^2$

$H \ll m$ the scalar field oscillates with frequency m, and a slow decay of the amplitude:

$$\phi = \phi_0(a/a_0)^{-3/2}\cos(mt)$$

➡ behaves like dark matter: $\rho \propto a^{-3}$

$V \propto \phi^n$ ➡ $w = \frac{\langle p_\phi\rangle}{\langle\rho_\phi\rangle} = \frac{n-2}{n+2}$

Brax et al. 2019

➡ For a mostly quadratic potential with small self-interactions:

$$V(\phi) = \frac{1}{2}m^2\phi^2 + V_{\rm I}(\phi) \qquad V_{\rm I} \ll \frac{1}{2}m^2\phi^2$$

$$\bar{\phi}(t) = \bar{\varphi}(t)\cos(mt - \bar{S}(t)) \qquad \bar{\varphi} = \bar{\varphi}_0 a^{-3/2} \qquad \bar{S}(t) = \bar{S}_0 - \int_{t_0}^{t} dt m\Phi_{\rm I}\left(\frac{m^2\bar{\varphi}_0^2}{2a^3}\right)$$

IV- Quartic self-interaction

Fuzzy Dark Matter (FDM) + self-interactions

$$S_\phi = \int d^4x\sqrt{-g}\left[-\frac{1}{2}g^{\mu\nu}\partial_\mu\phi\partial_\nu\phi - V(\phi)\right]$$

$$V(\phi) = \frac{m^2}{2}\phi^2 + V_{\rm I}(\phi) \quad \text{with} \quad V_{\rm I}(\phi) = \frac{\lambda_4}{4}\phi^4, \quad \lambda_4 > 0$$

$\rho \propto a^{-3}$

Repulsive self-interaction → Effective pressure

→ One characteristic density / length-scale:

$$\rho_a = \frac{4m^4}{3\lambda_4}, \quad r_a = \frac{1}{\sqrt{4\pi\mathcal{G}\rho_a}}$$

Relativistic regime - strong self-interaction

Jeans length - Radius of solitons

Very large occupation numbers: $N \sim \dfrac{\rho}{mp^3} \gg 1$ $\qquad m \ll 1\ \text{eV}$

De Broglie wavelength: $\lambda_{\rm dB} = \dfrac{2\pi}{mv} \lesssim 1\ \text{kpc}$ $\qquad m \gtrsim 10^{-22}\ \text{eV}$

Also, k-essence models: $S_\phi = \int d^4x\sqrt{-g}\left[\Lambda^4 K(X) - \dfrac{m^2}{2}\phi^2\right]$ $\qquad X = -\dfrac{1}{2\Lambda^4}g^{\mu\nu}\partial_\mu\phi\partial_\nu\phi$ $\qquad K(X) = X + K_{\rm I}(X)$

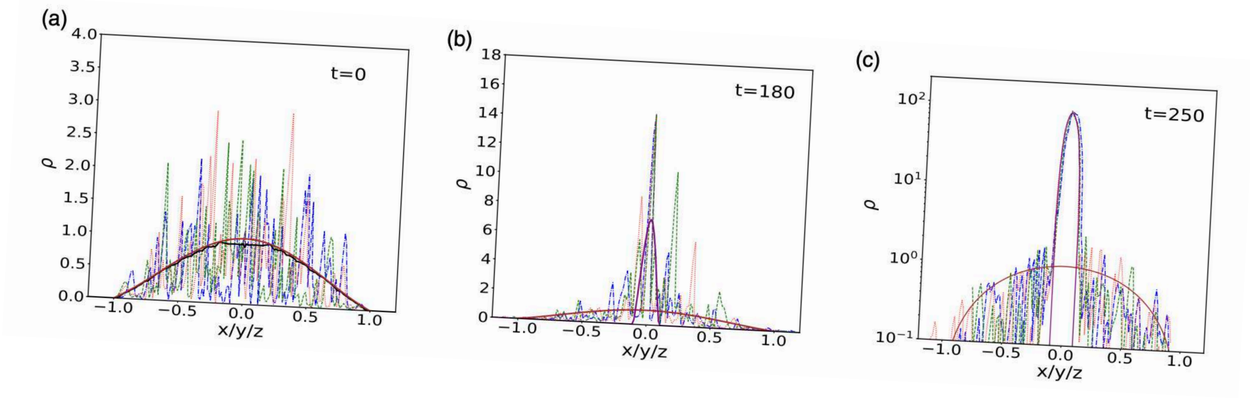

Galaxy-scale dynamics:

Formation of DM halos with a flat core

arXiv: 2304.1022, 2412.02519

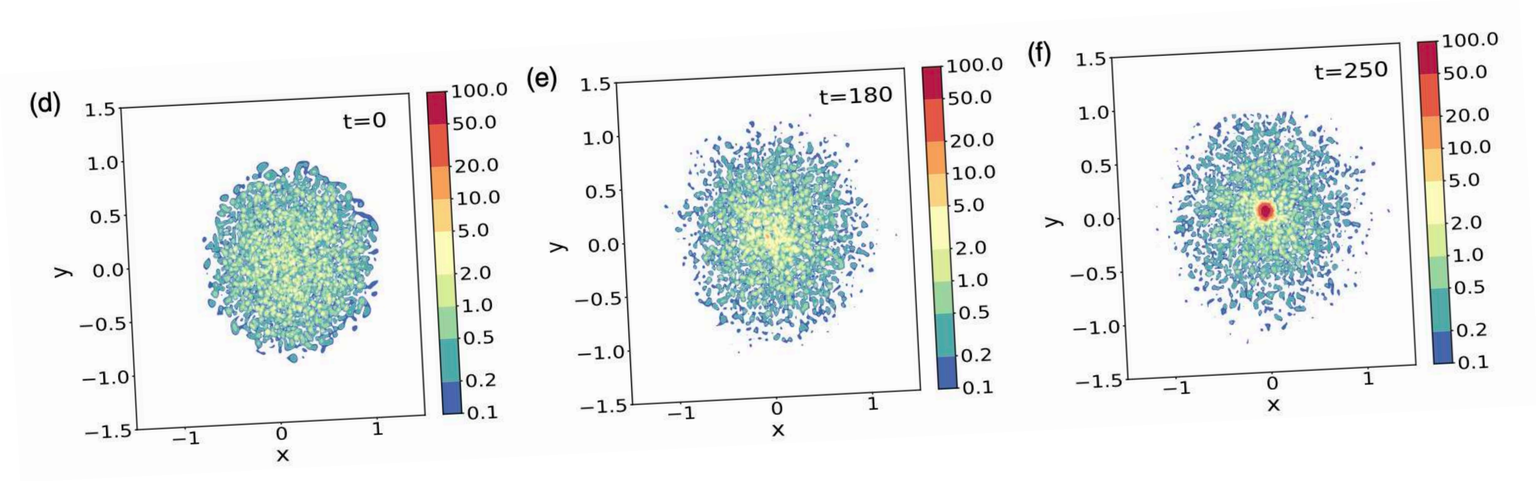

I- NON-RELATIVISTIC REGIME

On the scale of the galactic halo we are in the nonrelativistic regime: the frequencies and wave numbers of interest are much smaller than m and the metric fluctuations are small.

A) From Klein-Gordon eq. to (nonlinear) Schrödinger eq.:

Decompose the real scalar field ϕ in terms of the complex scalar field ψ

$$\phi = \frac{1}{\sqrt{2m}}(e^{-imt}\psi + e^{imt}\psi^\star)$$

factorizes (removes) the fast oscillations of frequency m

$$\dot{\psi} \ll m\psi, \quad \nabla\psi \ll m\psi$$

$\psi(x,t)$ evolves slowly, on astrophysical or cosmological scales.

Instead of the Klein-Gordon eq., it obeys a (non-linear) Schrödinger eq.: a Gross-Pitaevskii equation

$$i\left(\dot{\psi} + \frac{3}{2}H\psi\right) = -\frac{\nabla^2\psi}{2ma^2} + m\Phi_{\rm N}\psi + \frac{\partial\mathcal{V}_{\rm I}}{\partial\psi^\star}$$

Gross-Pitavskii equation: similar to BEC and superfluids at low temperature, where the external confining potential is replaced by the self-gravity.

Newtonian gravitational potential

self-interactions

$$V_{\rm I}(\phi) = \Lambda^4\sum_{p\geq 3}\frac{\lambda_p}{p}\left(\frac{\phi}{\Lambda}\right)^p$$

$$\mathcal{V}_{\rm I}(\psi,\psi^\star) = \Lambda^4\sum_{p\geq 2}\frac{\lambda_{2p}}{2p}\frac{(2p)!}{(p!)^2}\left(\frac{\psi\psi^\star}{2m\Lambda^2}\right)^p$$

(keep only even terms)

Inside galactic halos, we neglect the Hubble expansion:

Newtonian gravity

Self-interactions

$$i\dot{\psi} = -\frac{\nabla^2\psi}{2m} + m(\Phi_{\rm N} + \Phi_{\rm I})\psi$$

$$V_{\rm I}(\phi) = \frac{\lambda_4}{4}\phi^4$$

$$\Phi_{\rm I} = \frac{m|\psi|^2}{\rho_a}$$

$$\nabla^2\Phi_{\rm N} = 4\pi\mathcal{G}\rho \qquad \rho = m|\psi|^2$$

B) From Schrödinger eq. to Hydrodynamical eqs (Madelung transformation):

Madelung 1927, Chavanis 2012, ...

One can map the Schrödinger eq. to hydrodynamical eqs.: $\psi = \sqrt{\frac{\rho}{m}}e^{is}$ $\vec{v} = \frac{\nabla s}{m}$

The real and imaginary parts of the Schrödinger eq. lead to the continuity and Euler eqs.:

$$\dot{\rho} + \nabla\cdot(\rho\vec{v}) = 0$$

conservation of probability for ψ → conservation of matter for ρ

$$\dot{\vec{v}} + (\vec{v}\cdot\nabla)\vec{v} = -\nabla(\Phi_{\rm Q} + \Phi_{\rm N} + \Phi_{\rm I})$$

Self-interactions

$$\Phi_{\rm I} = \frac{\rho}{\rho_a}$$

effective pressure $P_{\rm eff} \propto \rho^2$ $\gamma = 2$

« quantum pressure » $\Phi_{\rm Q} = -\frac{\nabla^2\sqrt{\rho}}{2m^2\sqrt{\rho}}$

comes from part of the kinetic terms in ψ

In the following, we neglect the « quantum pressure » (which dominates for FDM) large-*m* limit

II- SOLITON (ground state): HYDROSTATIC EQUILIBRIUM

As compared with CDM, the self-interactions allow the formation of hydrostatic equilibrium solutions, with a balance between gravity and the effective pressure:

$$\cancel{\dot{\vec{v}}} + (\vec{v}\cdot\cancel{\nabla})\vec{v} = -\nabla(\cancel{\Phi_{\rm Q}} + \Phi_{\rm N} + \Phi_{\rm I}) \quad \rightarrow \quad \nabla(\Phi_{\rm N} + \Phi_{\rm I}) = 0 \quad \rightarrow \quad \rho(r) = \rho_0 \frac{\sin(r/r_a)}{(r/r_a)}$$

$$R_{\rm sol} \simeq \pi r_a$$

$$\rho_a = \frac{4m^4}{3\lambda_4}, \quad r_a = \frac{1}{\sqrt{4\pi \mathcal{G}\rho_a}}$$

Finite-size halo, called « soliton » or « boson star »

P. Brax, J. Cembranos, PV, 1906.00730

Ruffini and Bonazolla 1969,
Chavanis 2011,
Schiappacasse and Hertzberg 2018, ...

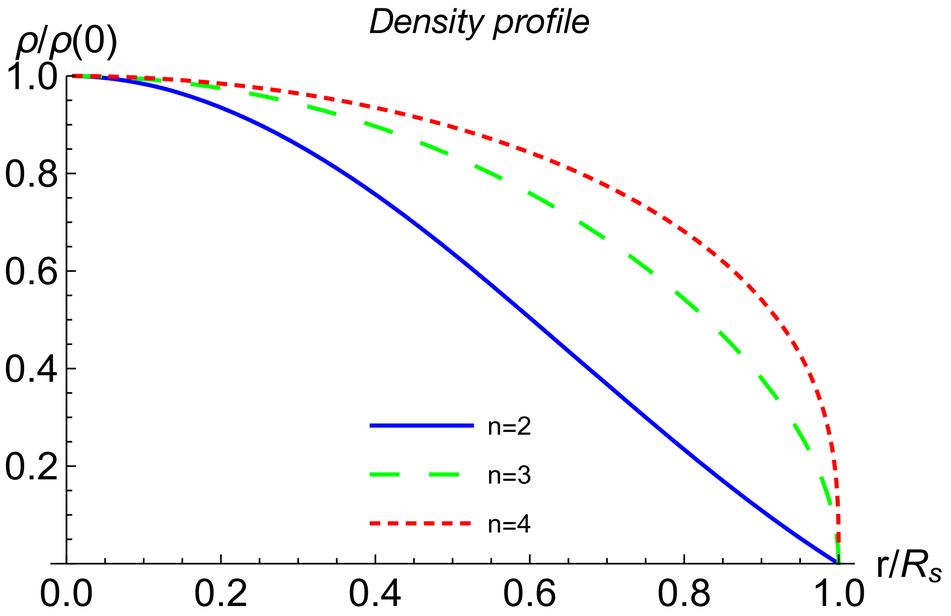

$$V_{\rm I}(\phi) = \Lambda^4 \frac{\lambda_{2n}}{2n} \frac{\phi^{2n}}{\Lambda^{2n}}$$

$m \gg 10^{-18}\mathrm{eV}$: galactic soliton governed by the balance between the repulsive self-interaction and self-gravity.

$m \sim 10^{-21}\mathrm{eV}$: Fuzzy Dark Matter (de Broglie wavelength of galactic size): galactic soliton governed by the balance between the quantum pressure and self-gravity.

Numerical simulations of FDM indeed find that solitons form, from gravitational collapse, within an extended NFW-like out-of-equilibrium halo.

Chen et al. 2020

Schive et al. 2014,
Veltmaat et al. 2018,
Mocz et al. 2019,
Amin and Mocz 2019, ...

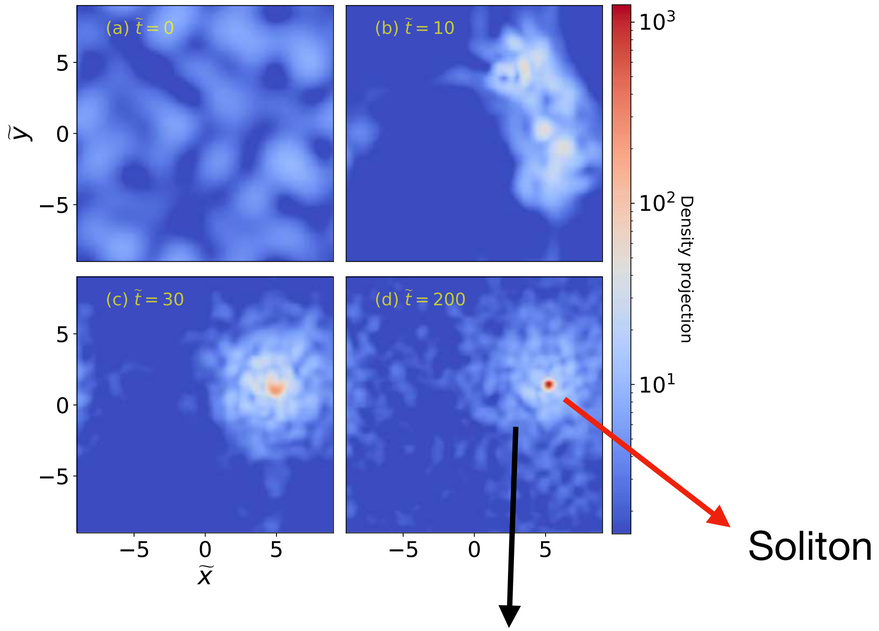

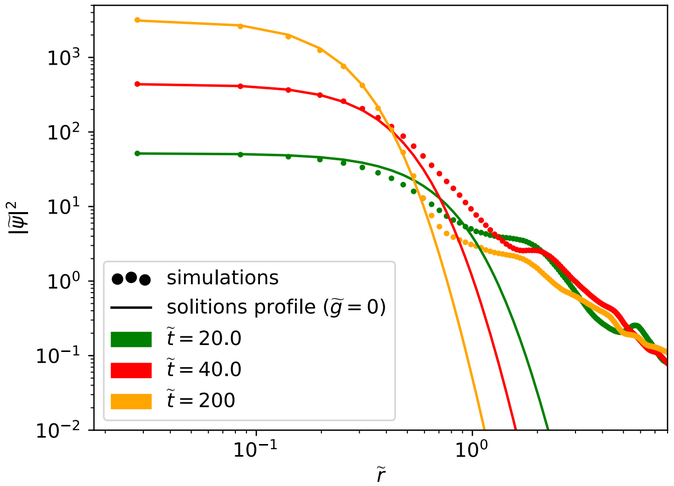

III- SOLITON FORMATION IN THE THOMAS-FERMI REGIME

(Self-interactions dominate over the quantum pressure in the soliton)

A) Numerical simulations

Initial conditions: halo (+ central soliton): $\psi_{\rm initial}=\psi_{\rm sol}+\psi_{\rm halo}$

$$\rho_{\rm sol}(r)=\rho_{0\rm sol}\frac{\sin(\pi r/R_{\rm sol})}{\pi r/R_{\rm sol}},\quad \hat{\psi}_{\rm sol}(r)=\sqrt{\rho_{\rm sol}(r)}$$

Stochastic halo: sum over eigenmodes of the target gravitational potential with random coefficients

$$\psi_{\rm halo}(\vec{x},t)=\sum_{n\ell m}a_{n\ell m}\hat{\psi}_{n\ell m}(\vec{x})e^{-iE_{n\ell}t/\epsilon}$$

$$a_{n\ell m}=a(E_{n\ell})e^{i\Theta_{n\ell m}}$$

random phase

$$-\frac{\epsilon^2}{2}\nabla^2\hat{\psi}_E+\bar{\Phi}\hat{\psi}_E=E\hat{\psi}_E\qquad \bar{\Phi}(r)=\bar{\Phi}_N(r),\quad \nabla^2\bar{\Phi}_N=4\pi\bar{\rho}$$

$$\langle\rho_{\rm halo}\rangle=\sum_{n\ell m}a(E_{n\ell})^2|\hat{\psi}_{n\ell m}|^2$$

Choose $a(E)$ so as to recover the target density profile $\rho(r)$

With the WKB approximation we can relate this system to a classical system defined by a phase-space distribution $f(E)$

take $a(E)^2=(2\pi\epsilon)^3 f(E)$

$$f(E)=\frac{1}{2\sqrt{2}\pi^2}\frac{d}{dE}\int_E^0\frac{d\Phi_N}{\sqrt{\Phi_N-E}}\frac{d\rho_{\rm classical}}{d\Phi_N}$$

(Eddington formula)

1) Soliton radius of the same order as the halo size: large self-interactions

Initial stochastic halo with a fixed mean density profile

Initial 1D density plot

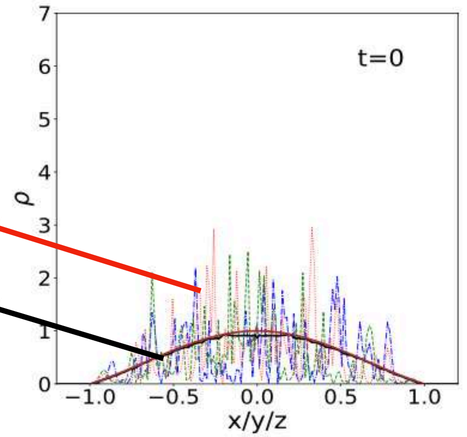

Initial 2D density plot

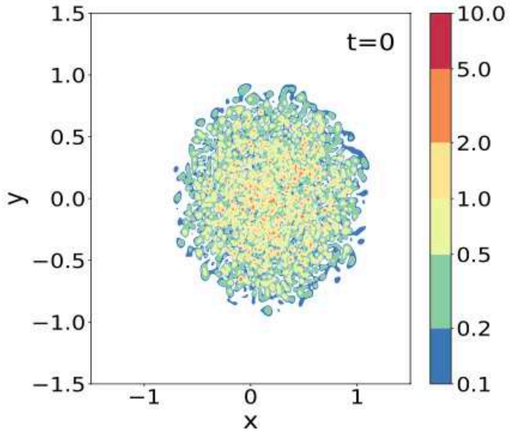

Final 1D density plot

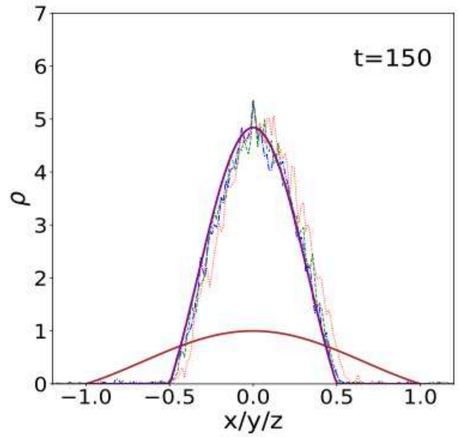

Final 2D density plot

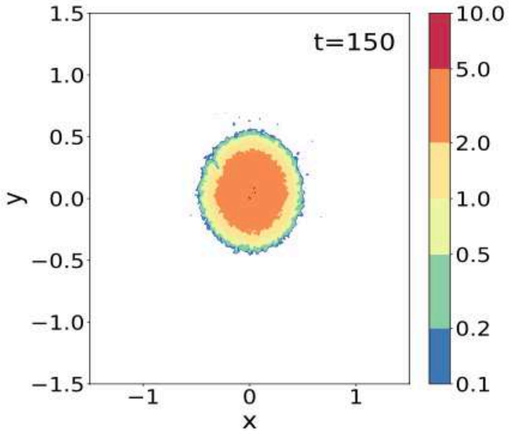

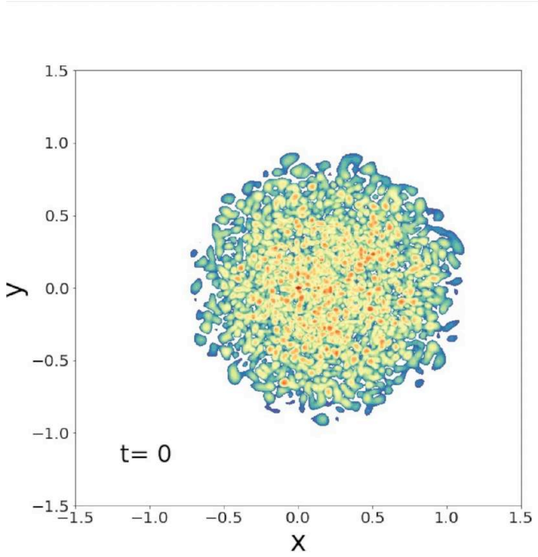

1D potential plot

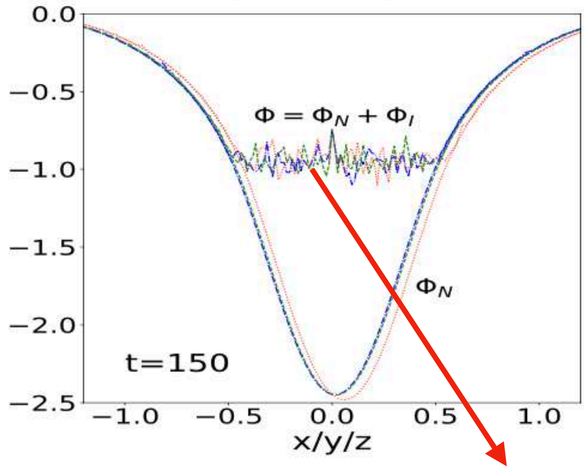

Evolution of total and soliton mass

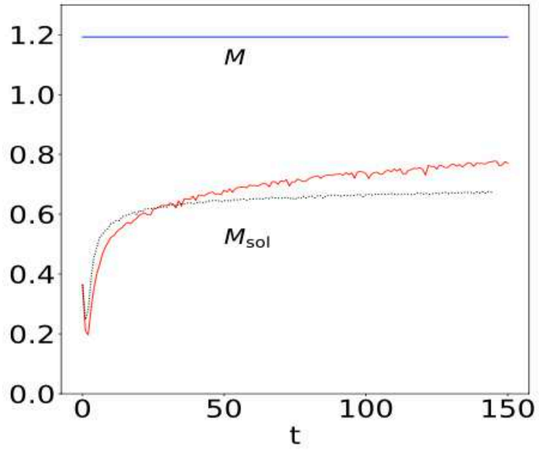

Evolution of energy components

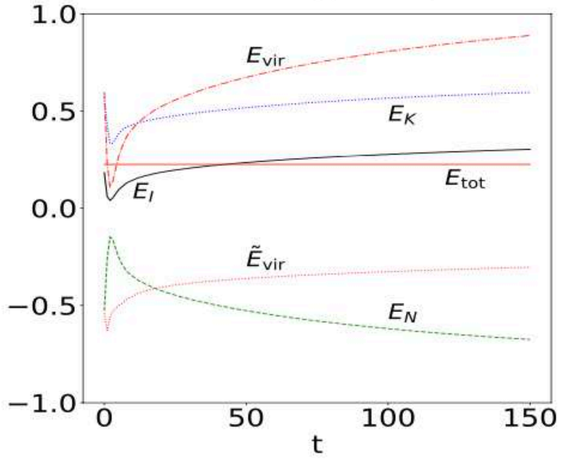

flat=soliton (hydrostatic eq.)

- At t ~ 8, the soliton is formed with Rsol ~ 0.5 and it contains ~ 50% of the total mass.
- The system reaches a quasi-stationary state.
- Afterwards, the soliton slowly grows.

2) Soliton radius much smaller than the halo size: small self-interactions

1D density plots

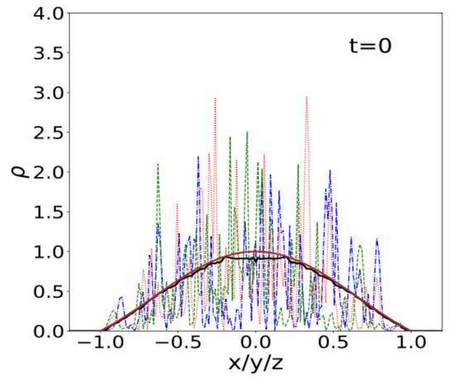

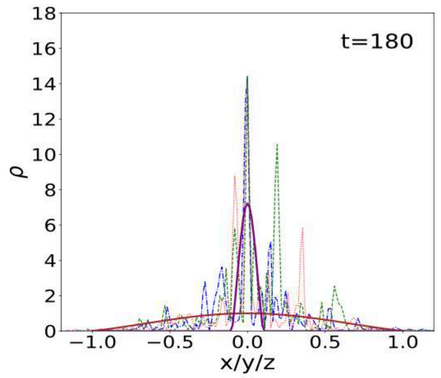

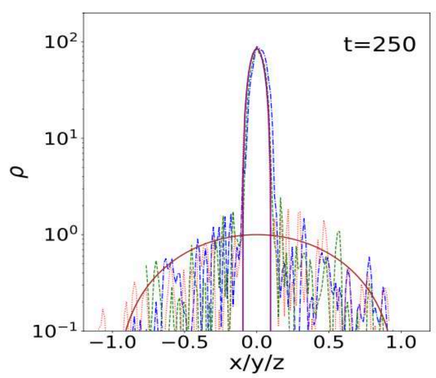

2D density plots

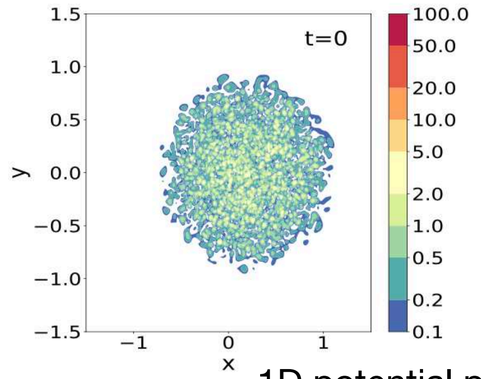

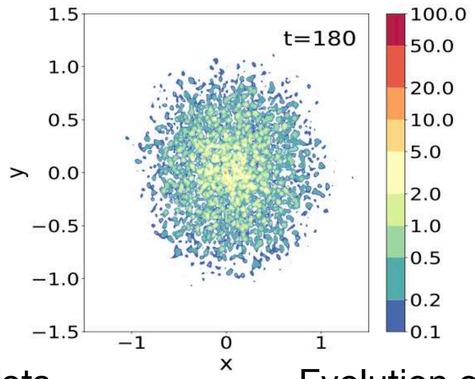

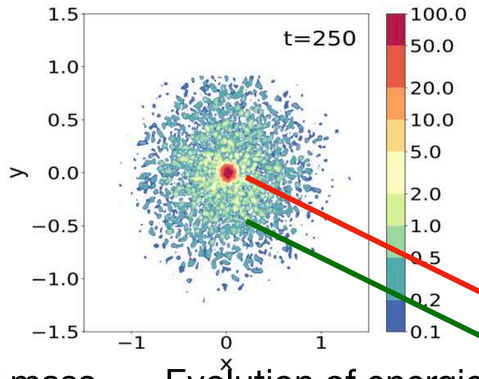

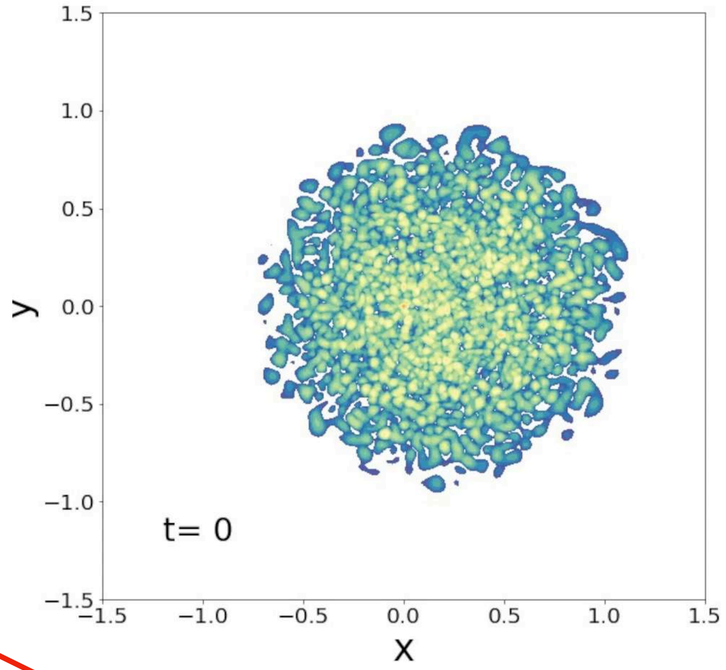

1D potential plots

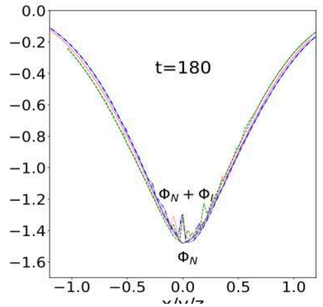

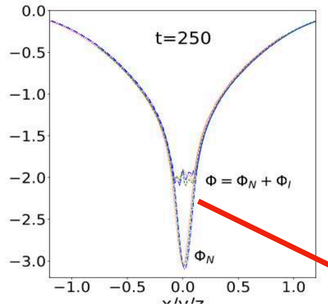

Evolution of mass

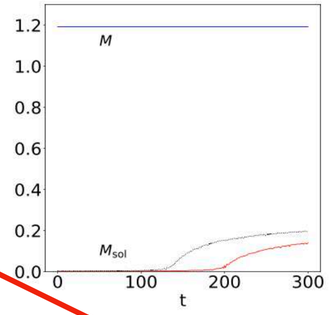

Evolution of energies

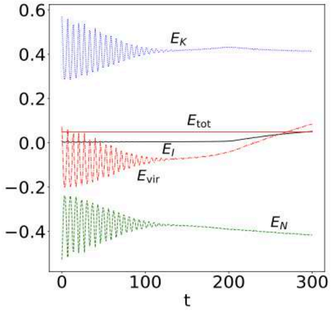

Central soliton

Stochastic halo (negligible self-interactions) dominated by kinetic terms and gravity (CDM - NFW)

flat=soliton

- By t ~ 100, the halo relaxes to a quasi-stationary state.
- At t ~180, FDM peak.
- At t ~ 200, self-interacting soliton forms, $R_{sol} = 0.1$.

Transition from a FDM phase to a self-interacting phase.

3) Dependence of the soliton mass on the formation history

Growth with time of the soliton mass

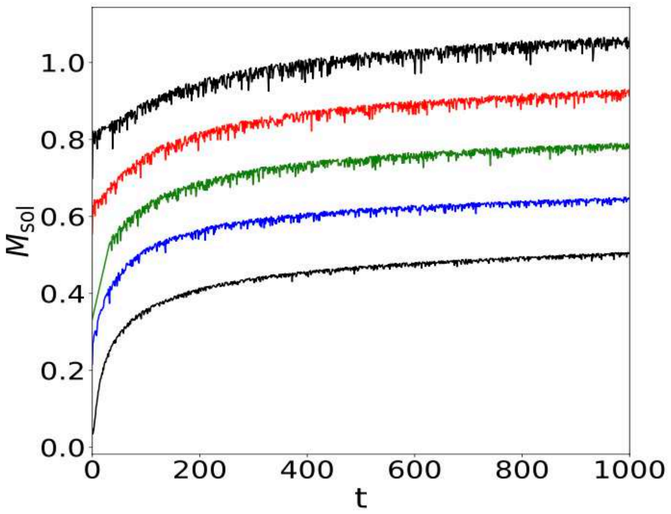

Growth rate as a function of the soliton mass, for several initial conditions

$$\Gamma_{\rm sol} = \frac{\dot{M}_0}{M_0}$$

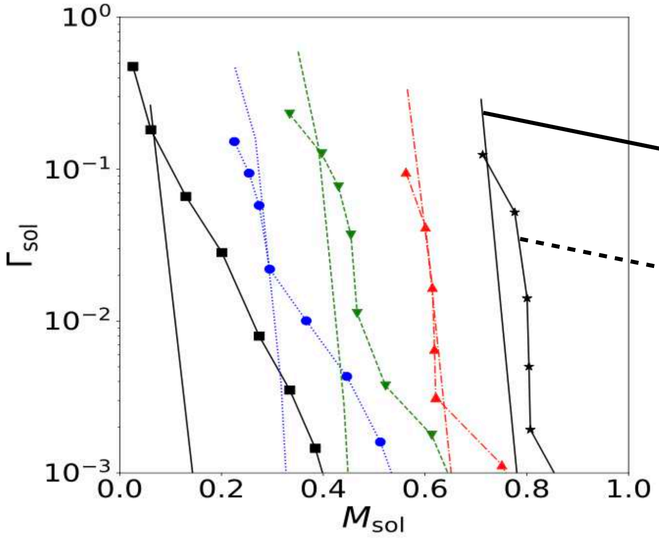

analytical model (kinetic theory)

numerical simulation

- The soliton always forms and grows, with a growth rate that decreases with time.
- Its mass can reach 50% of the total mass of the system.
- There is no sign of a scaling regime, where the growth rate would be independent of initial conditions.

→ Probably no well-defined halo-mass/soliton mass relation

IV- NON-POLYNOMIAL SELF_INTERACTION

$$\Phi_I(\rho) = \begin{cases} \rho/\rho_a & \text{if} \quad \rho < \rho_c \\ \rho_c/\rho_a & \text{if} \quad \rho > \rho_c \end{cases}$$

Transitions between self-interaction and quantum pressure euquilibrium.

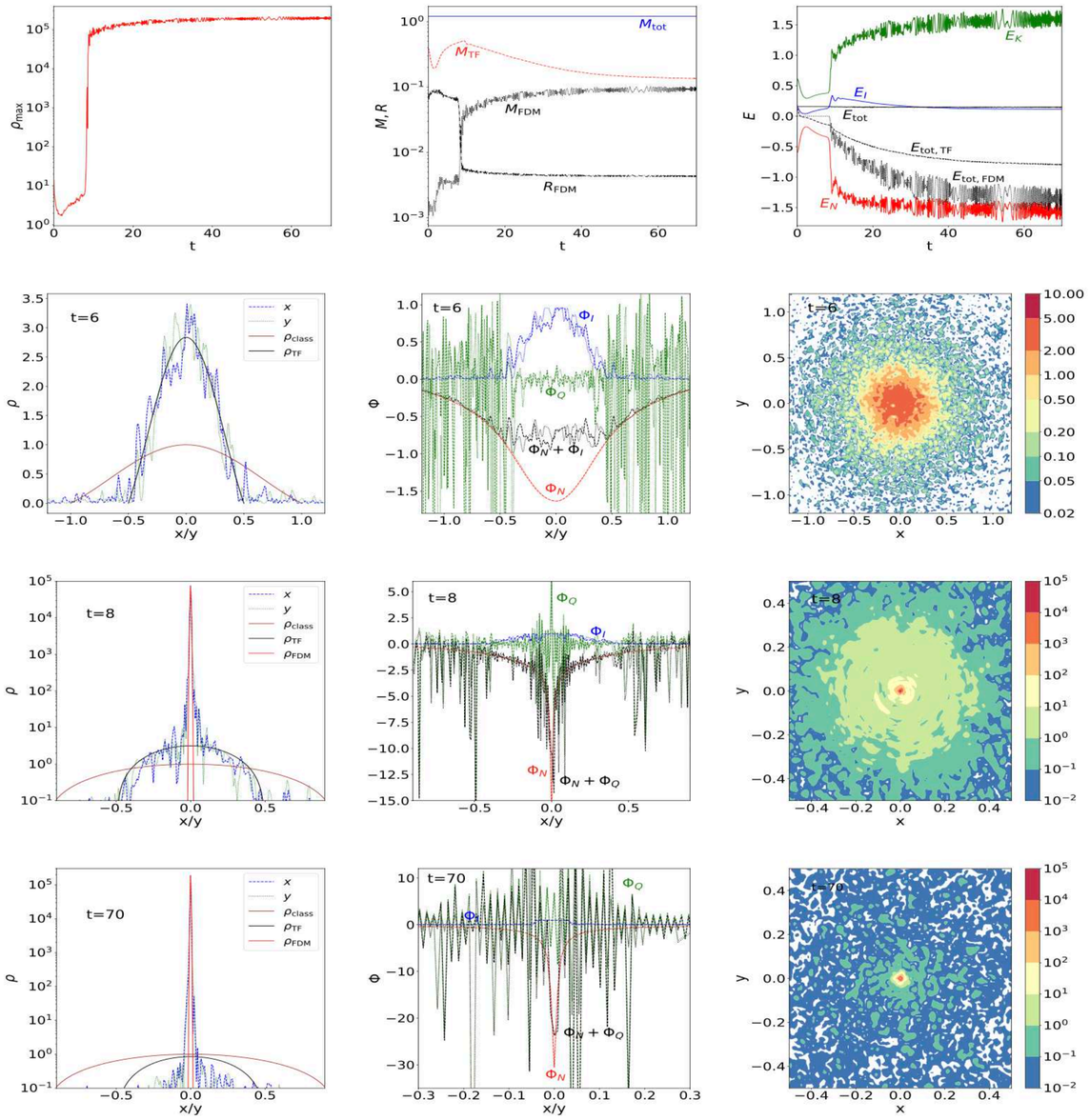

FIG. 4. Evolution of a halo with $R_{\rm TF} = 0.5$ and $\rho_c = 3$.

Solitons always form at the center of virialized halos.

For large self-interactions, the soliton forms in a few dynamical times.

For small self-interactions, the soliton formation can take a long time, until stochastic density peaks reach densities that are large enough to trigger the formation of the soliton.

The soliton keeps growing until the end of our simulations, making from 10% to 80% of the total mass.

The growth rate of the soliton does not seem to obey a scaling regime.
It seems to depend on the formation history of the system.

In the cosmological context, there should be a large scatter for the soliton mass as a function of the halo mass, depending on the assembly history ?

It is not clear how to derive simple but accurate analytical predictions for the soliton mass.

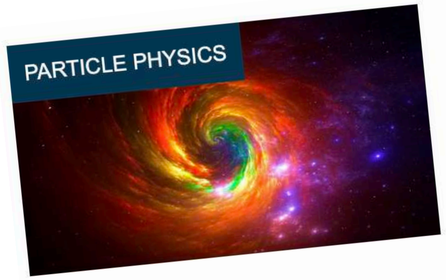

livescience.com

'A bundle of microscopic tornadoes' may be building the cosmic web

By Andrey Feldman published June 19, 2025

When invisible dark matter spins, it may form clumps of "vortexes" that stretch across space, forming the cosmic web that links all galaxies, new research proposes.

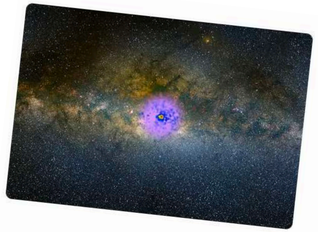

dailygeekshow.com

La matière noire ne serait pas une masse morte mais un superfluide ondulant et organisé dans l'univers

13 novembre 2025

Invisible, insaisissable, omniprésente : la matière noire fascine autant qu'elle frustre les scientifiques. Pourtant, une hypothèse bouscule tout. Et si cette composante mystérieuse n'était pas une mer glaciale de particules muettes, mais un superfluide quantique vibrant ? Une matière ondulatoire, dynamique, qui façonnerait les galaxies.

Vortex lines and rotating solitons

arXiv: 2501.02297, 2502.12100

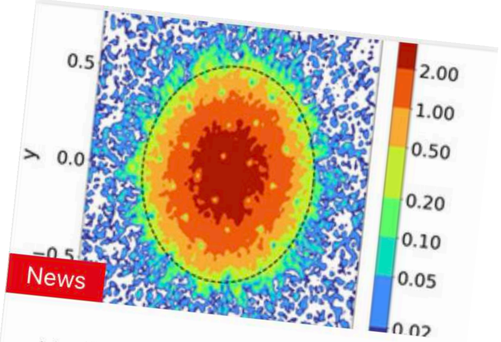

News

Vortices in Ultralight Dark Matter Halos

IPhT

10/13/2025

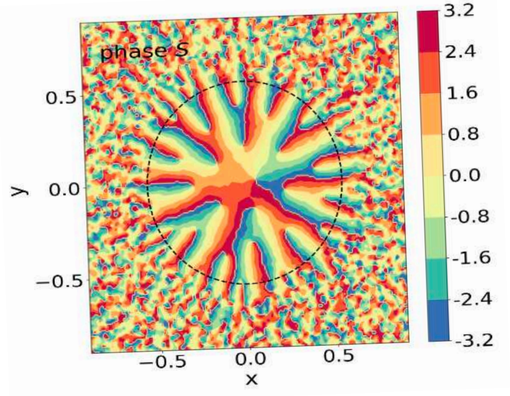

La première simulation de la formation de tourbillons dans des halos de matière noire ultralégère

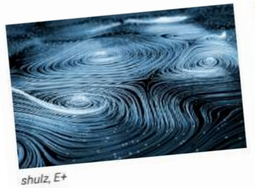

shulz, E+

Des chercheurs de l'IPhT (CEA, CNRS) ont étudié et simulé un modèle de matière noire dans l'hypothèse où elle serait constituée de particules élémentaires très légères. Grâce à des simulations numériques, les physiciens ont suivi la formation de larges structures en rotation (qui pourraient atteindre des dimensions galactiques) et observé l'apparition de tourbillons en leur sein, comme dans les superfluides étudiés en laboratoire. Ce phénomène, nouveau dans ce contexte, pourrait contribuer à lever le voile sur la nature de la matière noire, qui reste l'une des interrogations majeures de la cosmologie.

I- Vortices

(What happens when a collapsing halo has a nonzero angular momentum)

Nondimensional units (rescaled to the typical size and mass of the system)

$$i\epsilon\frac{\partial\psi}{\partial t} = -\frac{\epsilon^2}{2}\Delta\psi + (\Phi_N + \Phi_I)\psi \qquad \epsilon = \lambda_{dB}/L$$

$$\Delta\Phi_N = 4\pi\rho, \quad \Phi_I = \lambda\rho, \quad \rho = |\psi|^2 \qquad \epsilon \ll 1$$

→ Gross-Pitavskii equation: similar to BEC and superfluids at low temperature, where the external confining potential is replaced by the self-gravity.

Hydrodynamical picture: $\psi = \sqrt{\rho}e^{iS}, \quad \vec{v} = \epsilon\vec{\nabla}S$ → Curl-free velocity field

No longer true if the phase is not regular: at locations where the density vanishes this mapping is ill-defined !

→ Appearance of vortices/vortex lines that carry the vorticity of the system (BEC, superfluids). Associated with singularities of the phase and of the velocity field.

This is observed in cold atoms experiments: Abo-Shaer et al. 2001 (ballistic expansion after the trap is switched off)

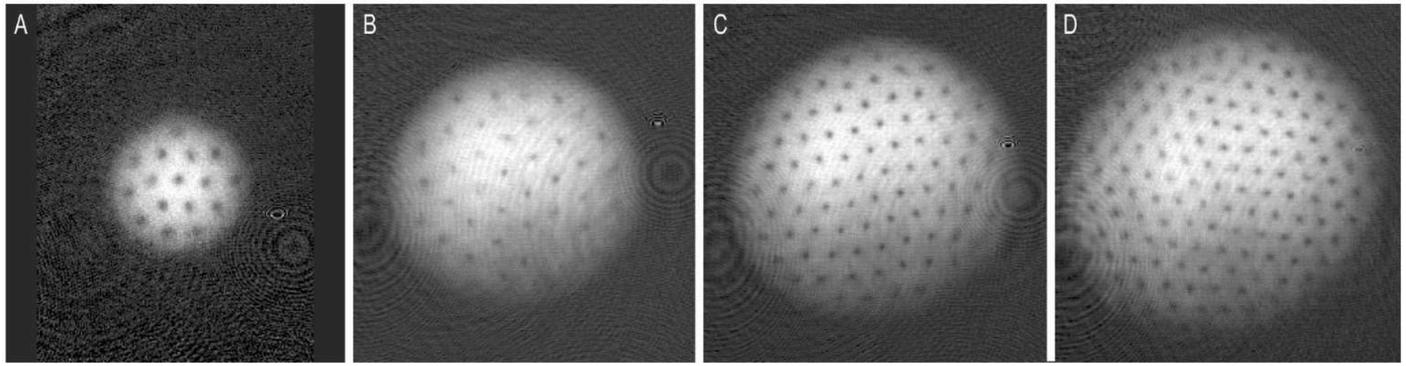

Fig. 1. Observation of vortex lattices. The examples shown contain approximately (**A**) 16, (**B**) 32, (**C**) 80, and (**D**) 130 vortices. The vortices have "crystallized" in a triangular pattern. The diameter of the cloud in (D) was 1 mm after ballistic expansion, which represents a magnification of 20. Slight asymmetries in the density distribution were due to absorption of the optical pumping light.

10^7 Na atoms Thomas-Fermi radius= $29\mu m$ Healing length $\xi = 0.2\mu m$

The spatial distribution of the density is obtained by resonant absorption imaging.

Rotation of the BEC is produced by the dipole force exerted by laser beams.

The vortices correspond to troughs of the density field.

One observes a regular lattice of vortices. Such Abrikosov lattices were first predicted for quantized magnetic flux lines in type-II superconductors. Abrikosov 1957

In our case, there is no external container.

→ The rotation will be generated by the initial rotation of the dark matter halo.

Axisymmetric case:

$$\psi(\vec{r},t) = e^{-i\mu t/\epsilon}\sqrt{\rho_0} f(r_\perp) e^{i\sigma\varphi}, \quad \rho(\vec{r}) = \rho_0 f^2(r_\perp)$$

Vortex line aligned with the vertical *z*-axis of integer spin σ

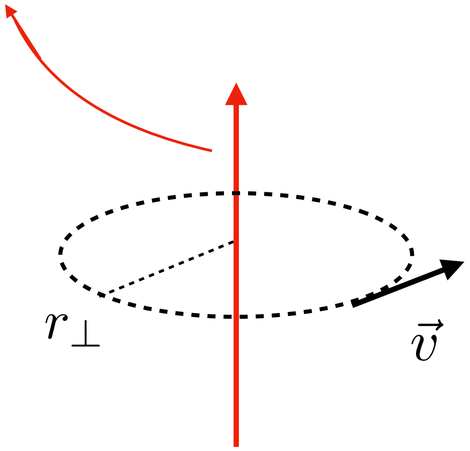

radial profile

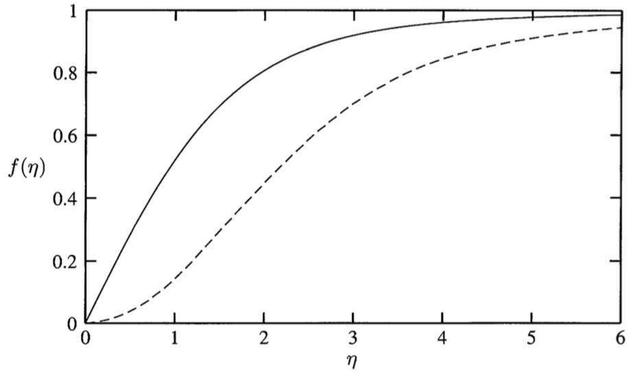

Pitaevski 2003

FIG. 5.2. Vortical solutions ($s = 1$, solid line; $s = 2$, dashed line) of the Gross–Pitaevskii equation as a function of the radial coordinate r/ξ. The density of the gas is given by $n(\boldsymbol{r}) = nf^2$, where n is the density of the uniform gas

Healing length: $\xi = \dfrac{\epsilon}{\sqrt{2\lambda\rho_0}}$ $\qquad r_\perp \ll \xi: \quad f \propto (r/\xi)^{|\sigma|}, \quad r_\perp \gg \xi: \quad f \simeq 1 - \dfrac{\sigma^2\xi^2}{2r^2} + \ldots$

Velocity field: $\vec{v} = \dfrac{\epsilon\sigma}{r_\perp}\vec{e}_\varphi = \epsilon\sigma\dfrac{\vec{e}_z \times \vec{r}_\perp}{r_\perp^2}, \quad v_{r_\perp} = v_z = 0, \quad v_\varphi = \dfrac{\epsilon\sigma}{r_\perp}$

The vorticity is carried by the vortices $\quad \vec{\omega} = \vec{\nabla} \times \vec{v} = 2\pi\epsilon\sigma\delta_D^{(2)}(\vec{r}_\perp)\vec{e}_z$

The vorticity and circulation are quantized $\quad \Gamma(r_\perp) = \oint_{\mathcal{C}} \vec{v}\cdot d\vec{\ell} = \int_S \vec{\omega}\cdot d\vec{S} = 2\pi\epsilon\sigma$

The excess energy (as compared with the static soliton) grows with the spin: $\Delta E_\sigma \sim \sigma^2 \pi \rho_0 \epsilon^2 \ln(R_0/\xi)$

It is energetically favorable for a large-spin vortex to break up into $|\sigma|$ unit-spin vortices.

In the numerical simulations we only find unit-spin vortices.

II- Many vortices

For a collection of N_v vortices: $\psi(\vec{r},t) = \sqrt{\rho} e^{is} \prod_{j=1}^{N_v} e^{i\sigma_j \varphi_j}$ $\varphi_j(\vec{r}) = \widehat{(\vec{e}_x, \vec{r}_\perp - \vec{r}_{\perp j})}$

As in classical hydrodynamics of ideal fluids, the vortices move with the matter along the flow generated by the other vortices and the background curl-free velocity

$$\dot{\vec{r}}_i = \vec{v}(\vec{r}_i), \quad \vec{v} = \epsilon \vec{\nabla} s + \sum_{j=1}^{N_v} \vec{v}_j$$

The system is again described by the continuity and Euler equations, but the velocity field is no longer curl-free:

$$\vec{\omega} = \vec{\nabla} \times \vec{v} = 2\pi\epsilon \vec{e}_z \left(\sum_j \sigma_j \delta_D^{(2)}(\vec{r}_\perp - \vec{r}_{\perp j}) \right)$$

III- Continuum limit

The Gross-Pitaevskii equation conserves the mass, the momentum and the energy, as well as the angular momentum.

Rotating soliton: we look for a minimum of the energy at fixed mass and angular momentum: $\delta^{(1)}\left(E-\mu M-\Omega J_z\right)=0$

Lagrange multipliers

→ Solid-body rotation: $\vec{v}=\vec{\Omega}\times\vec{r}$ $\qquad \vec{\Omega}=\Omega\,\vec{e}_z$

At leading order for a slow rotation, we obtain the density profile and the soliton surface:

$$\rho(r,\theta)=\left(\rho_0-\frac{\Omega^2}{2\pi}\right)j_0\left(\frac{\pi r}{R_0}\right)-\frac{5\pi\Omega^2}{12}j_2\left(\frac{\pi r}{R_0}\right)P_2(\cos\theta)+\frac{\Omega^2}{2\pi},$$

$$R_\Omega(\theta)=R_0\left(1+\frac{\Omega^2}{2\pi\rho_0}\right)-R_0\frac{5\Omega^2}{4\pi\rho_0}P_2(\cos\theta)$$

→ Oblate shape: $\qquad R_z=R_0\left(1-\frac{3\Omega^2}{4\pi\rho_0}\right)$ $\qquad R_{xy}=R_0\left(1+\frac{9\Omega^2}{8\pi\rho_0}\right)$ $\qquad R_{xy}>R_z$

→ Dynamical stability for $\qquad |\Omega|\lesssim\sqrt{\rho_0}$ $\qquad \Phi_{\rm rot}\lesssim\Phi_N\sim\Phi_I$

IV- Numerical simulations

A) Initial conditions

$J_{z\mathrm{init}} \simeq 0.17$

Density along the x/y/z axis

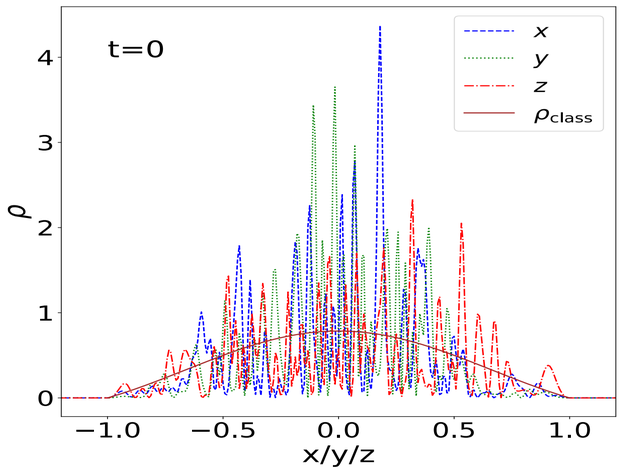

Density

Phase

Equatorial (x,y) plane

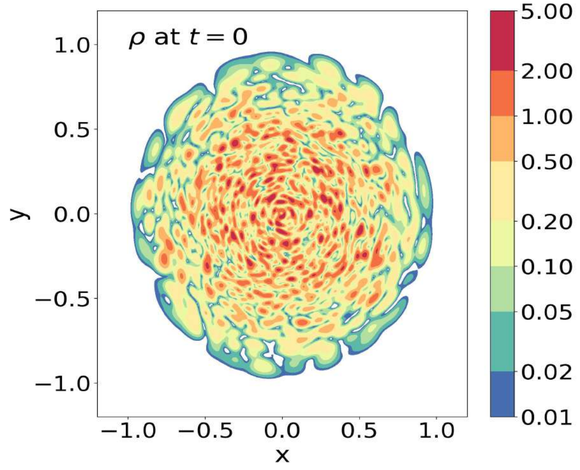

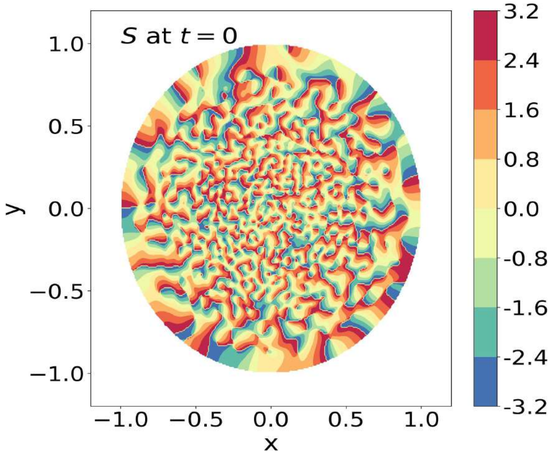

Vertical (x,z) plane

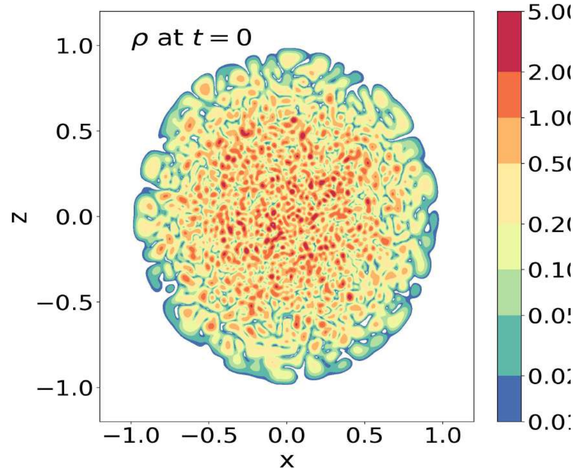

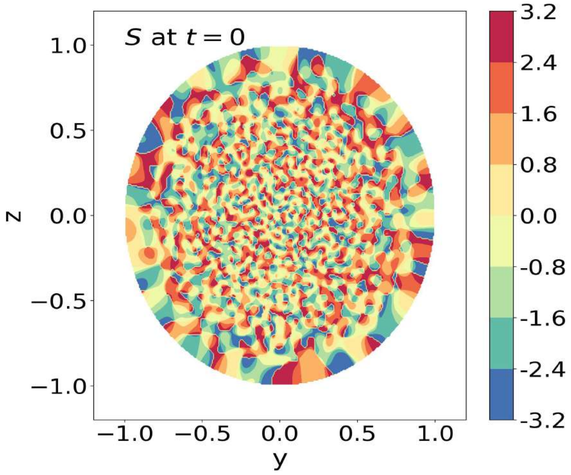

B) Formation of a rotating soliton in a few dynamical times

Mass and Density

Mass

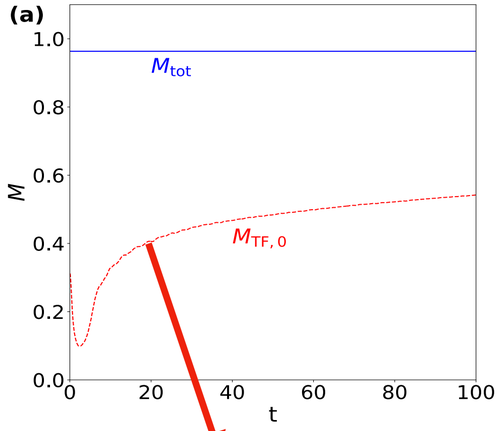

Growth of the soliton mass

Density

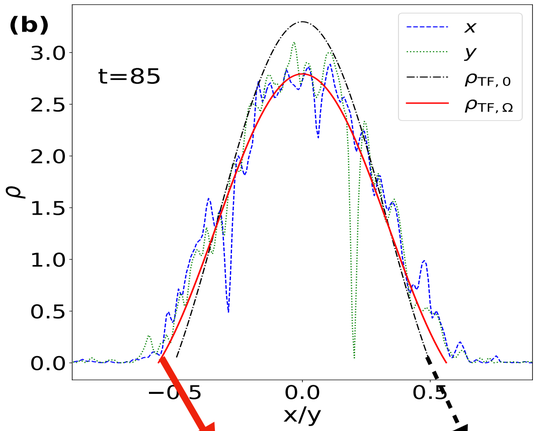

Rotating soliton profile

Static soliton profile

Density

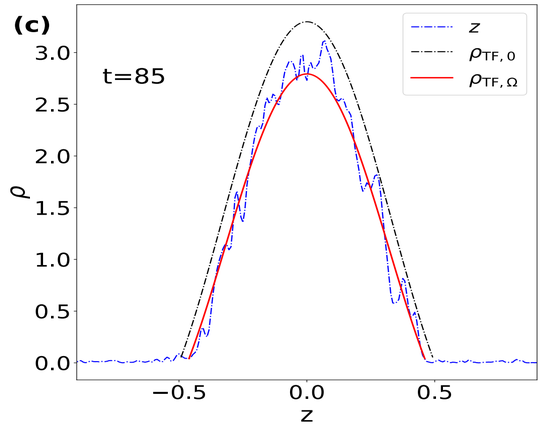

Velocity

Radial velocity in the equatorial plane

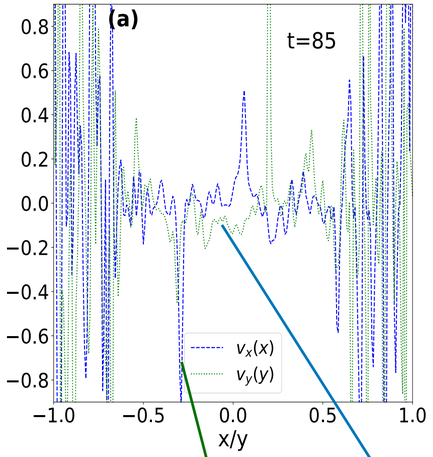

Vertical velocity in the equatorial plane

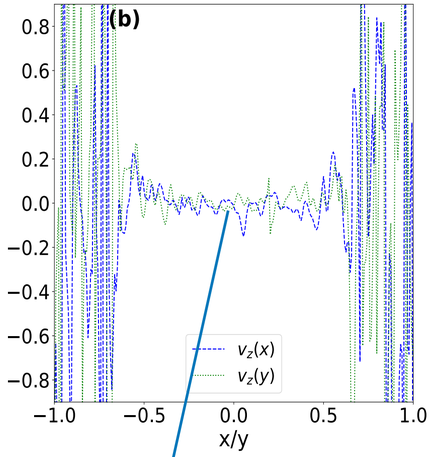

Other velocity components fluctuate around zero

Transverse horizontal velocity in the equatorial plane

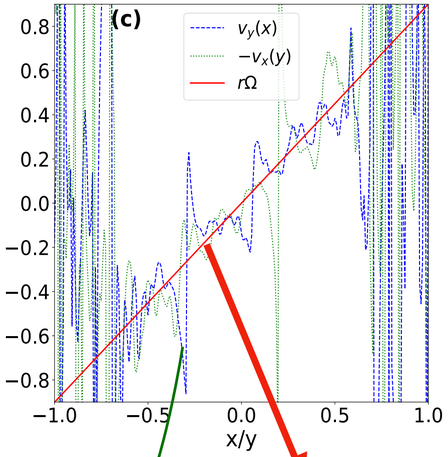

Solid-body rotation

$v_\perp = \Omega r_\perp$

The three velocity components along the vertical axis

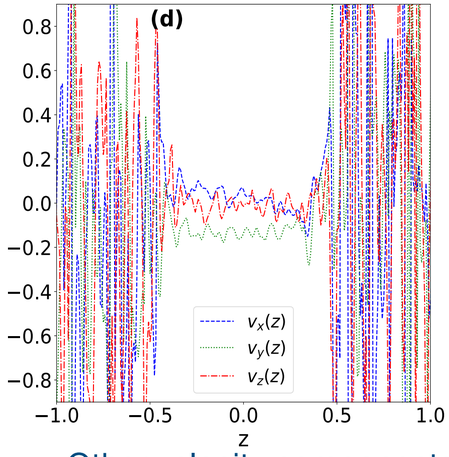

Other velocity components fluctuate around zero

Divergences due to the vortex lines

Circular section of the soliton

Lattice of velocity troughs

Density

Phase

Winding number

Random vortices of +/- spin in the outer virialized halo

Regular lattice of vortex lines inside the soliton

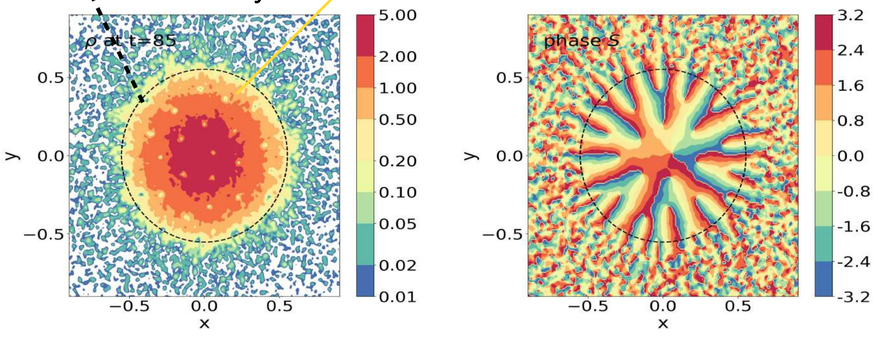

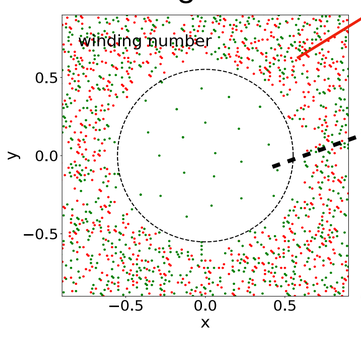

Equatorial (x,y) plane

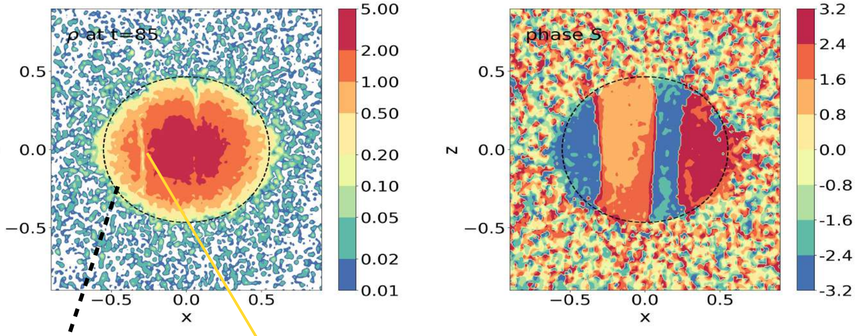

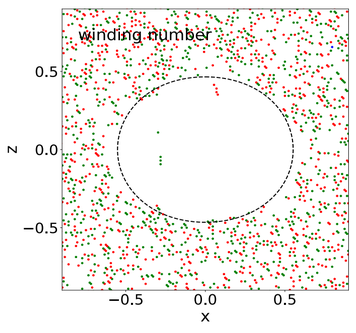

Vertical (x,z) plane

Oblate shape of the rotating soliton

Trace of a vertical vortex line

Solid-body rotation inside the soliton

Divergent velocity on the vortices

Normalised velocity

Streamlines

Velocity amplitude

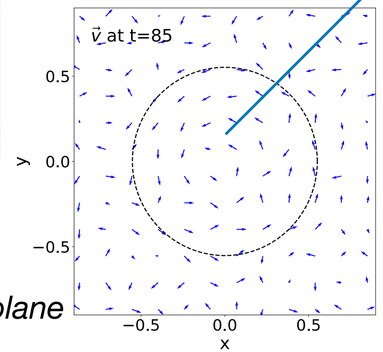

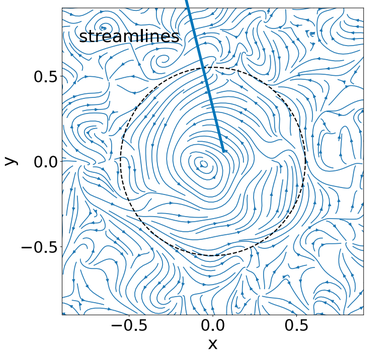

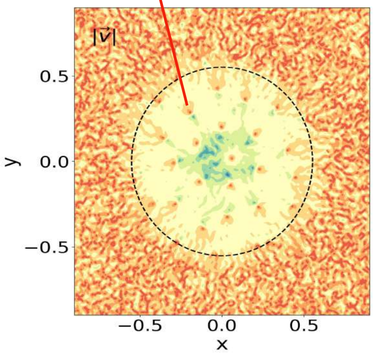

Equatorial (x,y) plane

Velocity fluctuates around zero inside the vertical plane

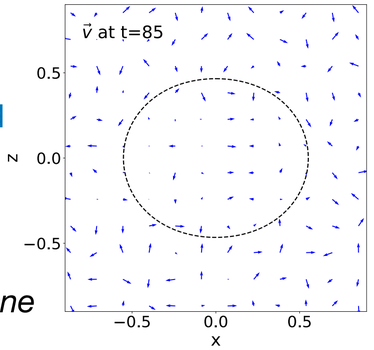

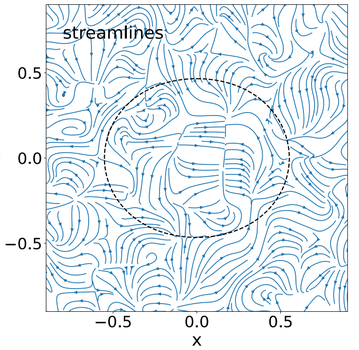

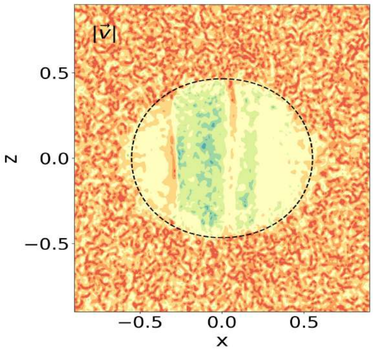

Vertical (x,z) plane

C) Formation of a lattice of vertical vortex lines

Vertical vortex lines inside the soliton

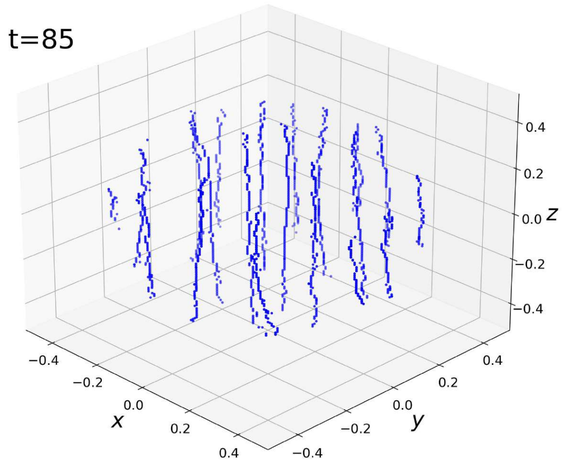

Projection onto the equatorial plane

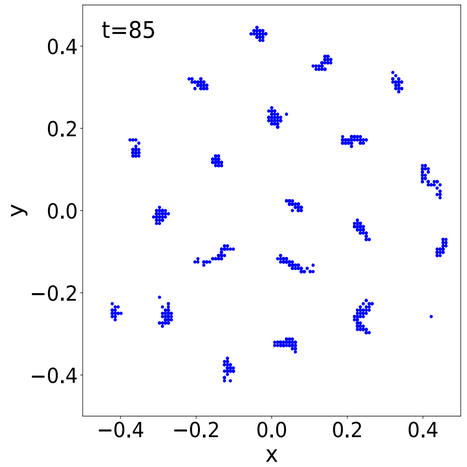

Projection onto the vertical plane

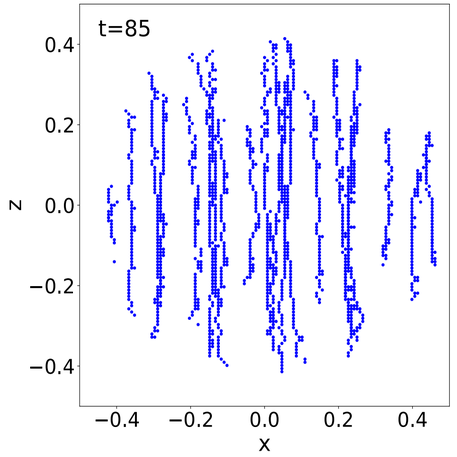

Stacking of the vortex lines (winding number maps) over many times

Solid-body rotation of the vortex lines in the equatorial plane

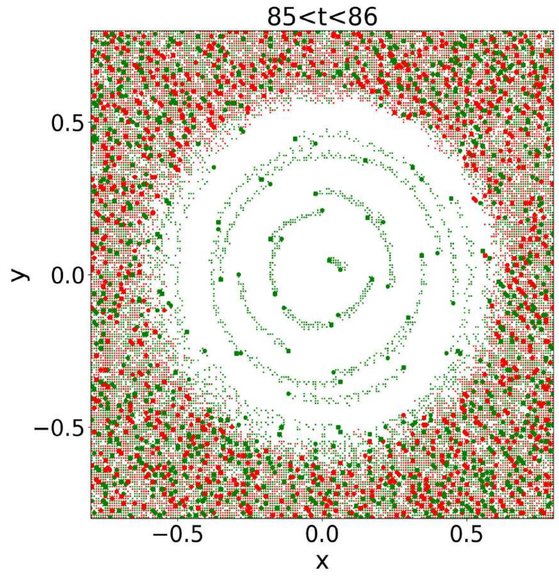

Trace of vertical vortex lines passing through the vertical plane

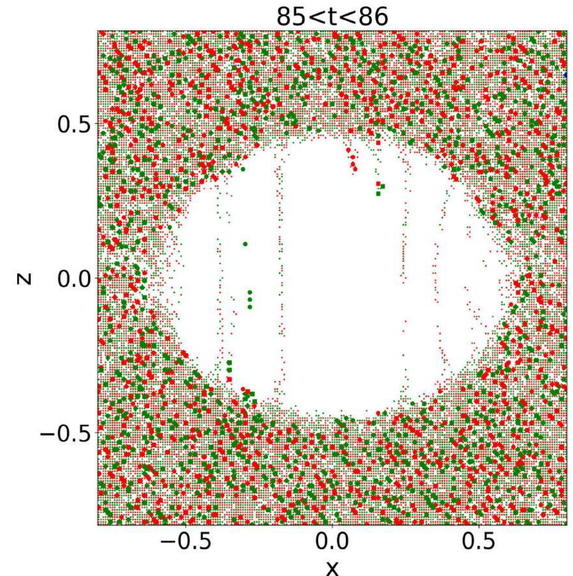

Halos with a nonzero angular momentum form stable rotating solitons with an oblate shape, for

These rotating solitons are not high angular momentum eigenstates of the Schrödinger equation with a vanishing central density

$$\psi_{\ell m}(\vec{x},t) = e^{-i\mu t/\epsilon} f(r) Y_\ell^m(\theta,\varphi) \qquad\qquad \ell \gg 1, \quad |m| \gg 1$$

Instead, they have a maximum central density and display a solid-body rotation that is supported by a regular lattice of vortex lines, aligned with the initial angular momentum of the system.

The number of vortex lines grows linearly with the soliton angular momentum.

- Cosmic web of vortex lines along filaments, linking collapsed halos ?

- Connection with spinning filaments ?

- Relativistic regime ? Frame dragging effects on baryons ?

- Detection of such DM substructures by lensing ?

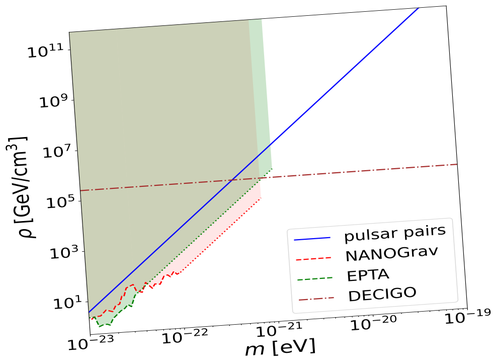

Detecting scalar dark matter clumps

with pulsar timing arrays

arXiv: 2506.08786

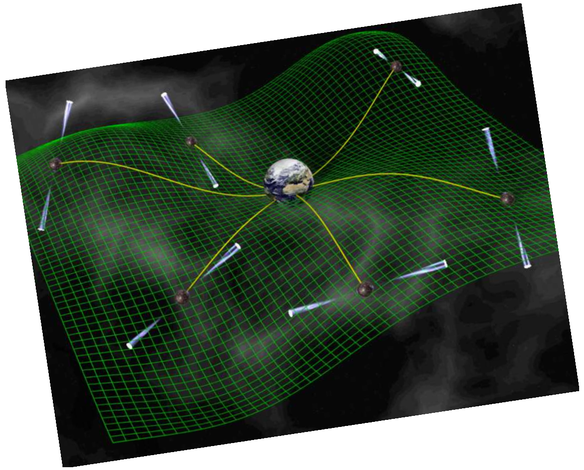

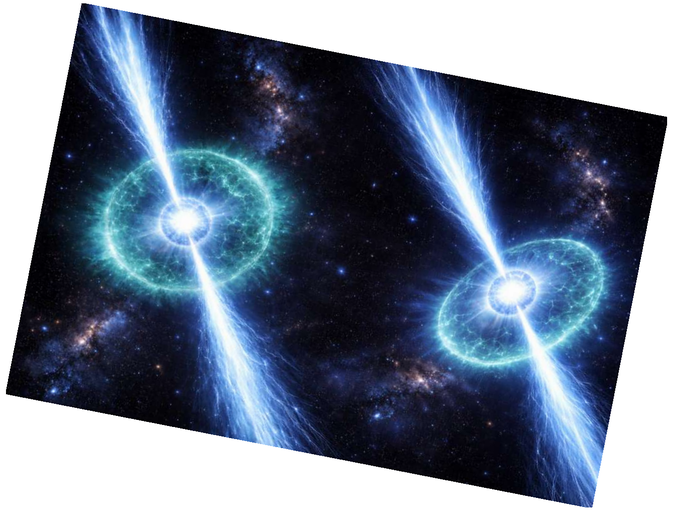

I- Oscillating term in the gravitational potential

In the non relativistic regime we obtained the solution in terms of a complex scalar field ψ with $\phi = \frac{1}{\sqrt{2m}}\left(e^{-imt}\psi + e^{imt}\psi^\star\right)$

which was solution of a nonlinear Schrödinger equation.

Going back to the scalar field ϕ which is solution of the Klein-Gordon eq. of motion, we obtain inside a soliton moving at velocity $\vec{v}_0$

$$\phi = \frac{\sqrt{2\rho}}{m}\cos(Et + \beta) \qquad \text{with} \qquad \beta = \alpha - m\vec{v}_0 \cdot \vec{x}$$

unknown offset

$$E = m(1+\mu) = m\left(1 + \frac{v_0^2}{2} + \Phi_Q + \Phi + \Phi_I\right)$$

kinetic energy

« quantum », gravitational and self-interaction potentials

This oscillating scalar field leads to subleading oscillating components in the energy-momentum tensor.

This also leads to subleading oscillating components in the gravitational potential: Khmelnitsky & Rubakov (2014)

$$\nabla^2\bar{\Psi} = 4\pi\mathcal{G}\rho_0, \qquad \Psi_{\rm osc} = \frac{\pi\mathcal{G}\rho_0}{m^2}\cos(2\theta) \qquad \text{with} \qquad \theta = Et + \beta \qquad R \gg 1/m$$

II- Sachs-Wolfe effect and time delay

As for the Sachs-Wolfe effect for the CMB, when photons travel from a pulsar toward the Earth their frequency is modified by the metric fluctuations:

$$\frac{f_e - f_p}{f_p} = \int_{t_p}^{t_e} dt\, \partial_t(\Phi + \Psi) + \Phi_p - \Phi_e$$

This gives rise to a time delay of the pulses measured on the Earth: $\delta t = \frac{\Psi_p}{2m} \sin(2E_p t + \gamma_p), \quad \gamma_p = -2E_p d_p + 2\beta_p$

(Here we neglect the integrated SW effect, damped by the oscillations, and we assume the gravitational potential is deeper around the pulsar than near the Earth)

Standard analysis use this result to search for ULDM signal in pulsar timing arrays, with $E_p \simeq m, \quad f = m/\pi$

$\Delta T_{\rm obs} \simeq 1$ week $\qquad f_{\rm max} \sim 1/\Delta T_{\rm obs} \sim 10^{-6}$ Hz $\qquad m_{\rm max} = \pi f_{\rm max} \sim 10^{-21}$ eV

Khmelnitsky & Rubakov (2014), Porayko et al. (EPTA) (2025), Afzal et al. (NANOGrav) (2024)

→ Rules out ULDM in the range: 10^{-24} eV $\lesssim m \lesssim 10^{-22}$ eV

→ Can one probe higher masses by cross-correlating the signals from different pulsars ?

III- Correlating 2 pulsars

Two pulsars $a,\ b$ with measurement times $t_{ai},\ t_{bj}$

$$\delta t_{ai}\delta t_{bj} = \frac{\Psi_a\Psi_b}{8m^2}\left[\cos(2E_a t_{ai} - 2E_b t_{bj} + \gamma_a - \gamma_b) - \cos(2E_a t_{ai} + 2E_b t_{bj} + \gamma_a + \gamma_b)\right]$$

$$\omega = 2(E_a - E_b) = 2m(\mu_a - \mu_b) \ll 2m \qquad \omega \simeq 4m$$

Introducing an oscillatory filter, we consider the observable:

$$s = \frac{1}{N_{ij}}\sum_{ij}\delta t_{ai}\delta t_{bj}\cos(4\omega\bar{t}_{ij}), \qquad \omega > 0$$

$$\bar{t}_{ij} = \frac{t_{ai}+t_{bj}}{2}, \quad \Delta t_{ij} = \frac{t_{ai}-t_{bj}}{2},$$

We consider the regime: $4mT_{\rm obs} \gg \pi, \quad 4m|\Delta t_{ij}| \ll \pi, \quad |m|\Delta\mu| - \omega|\, T_{\rm obs} \ll \frac{\pi}{8}$

which corresponds to: $m \gg \left(\frac{T_{\rm obs}}{1\,{\rm yr}}\right)^{-1} 2\times 10^{-23}\,{\rm eV}, \qquad m \ll \left(\frac{|\Delta t|}{1\,{\rm hour}}\right)^{-1} 10^{-19}\,{\rm eV}, \qquad |m|\Delta\mu| - \omega| \ll \left(\frac{T_{\rm obs}}{1\,{\rm yr}}\right)^{-1} 8\times 10^{-24}\,{\rm eV}.$

Move the mass window upward by correlating 2 pulsars measured at (almost) same time

IV- Signal-to-noise ratio

$$\delta\mathbf{t} = \mathbf{M}\cdot\epsilon + \mathbf{w} + \mathbf{r} + \delta\mathbf{t}_{\rm GW} + \delta\mathbf{t}_{\rm DM},$$

- $\mathbf{M}\cdot\epsilon$: error in the timing model (Earth orbit, …)
- $\mathbf{w}$: white noise
- $\mathbf{r}$: red noise
- $\delta\mathbf{t}_{\rm GW}$: stochastic GW background
- $\delta\mathbf{t}_{\rm DM}$: ULDM signal

Mean signal:

$$\overline{\langle s\rangle} = s_{\rm DM} + s_{\rm GW}$$

$$s_{\rm DM} = \frac{\Psi_a\Psi_b}{16m^2}\cos(2\Delta\gamma) = \frac{\pi^2\mathcal{G}^2\rho_a\rho_b}{16m^6}\cos(2\Delta\gamma)$$

$$\Delta\gamma = \frac{\gamma_a-\gamma_b}{2},\quad \gamma_p = -2E_p d_p + 2\beta_p.$$

$$s_{\rm GW} = \Gamma_{ab}\cos[2\omega(N+1)\Delta T]e^{-2\sigma^2\omega^2}\frac{\sin(2\omega T_{\rm obs})}{N\sin(2\omega\Delta T)}\int_{f_{\rm min}}^{f_{\rm max}} df\, P_{\rm GW}(f)e^{-2\pi^2\sigma^2 f^2}$$

- Γ_{ab}: Hellings & Downs
- $\frac{\sin(2\omega T_{\rm obs})}{N\sin(2\omega\Delta T)}$: damping

Variance:

$$\langle s^2\rangle_w = \frac{1}{N^2}\sum_i \cos^2(4\omega T_i)\sigma_{ai}^2\sigma_{bi}^2.$$

white noise

$$\sigma_r^2 = \overline{\langle s^2\rangle_r} = \frac{1}{2T_{\rm obs}}\int_{f_{\rm min}}^{f_{\rm max}} df\, P_a(f)P_b(f),$$

red noise, average over noise randomness and over measurement times

$$\sigma_{\rm GW}^2 = \frac{1+\Gamma_{ab}^2}{2T_{\rm obs}}\int_{f_{\rm min}}^{f_{\rm max}} df\, P_{\rm GW}(f)^2$$

→ stochastic GW background

Signal-to-noise ratio: $\mathrm{SNR} = \left| \frac{\langle s \rangle}{\sigma_s} \right|, \qquad \sigma_s^2 = \sigma_w^2 + \sigma_r^2 + \sigma_{\mathrm{GW}}^2.$

Detection requires a large DM density.

$\mathrm{SNR} > 1:$

$$\rho_{\mathrm{SNR}} > \frac{\sqrt{\sigma_s}}{10^{-7}\,\mathrm{s}} \left(\frac{m}{10^{-20}\,\mathrm{eV}} \right)^3 5 \times 10^9\,\mathrm{GeV/cm^3}$$

$$\rho_{\mathrm{SNR}} > \frac{\sqrt{\sigma_s}}{10^{-7}\,\mathrm{s}} \left(\frac{m}{10^{-20}\,\mathrm{eV}} \right)^3 3 \times 10^{15}\,\bar{\rho}_0$$

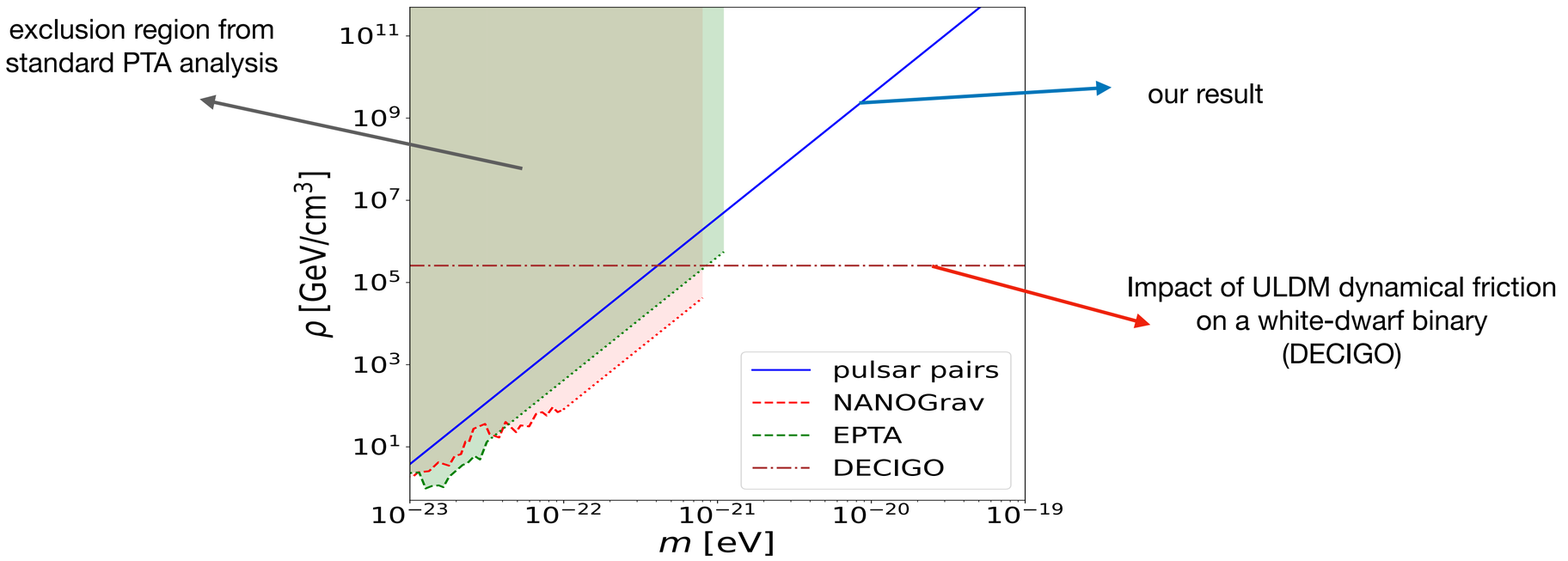

- As expected our analysis is somewhat less efficient than standard PTA analysis (only 1 pulsar pair).
- It can extend to higher mass.
- But at these higher masses other probes (gravitational waveforms) may be more efficient.
- Needs ULDM densities higher than the mean Milky Way DM density by a factor 10^6 at least.

V- Example / caveat

$$m = 10^{-20}\,\mathrm{eV}, \quad \rho = 5 \times 10^{9}\,\mathrm{GeV/cm^3}, \qquad R = 0.1\,\mathrm{pc}, \;\; \bar{\Psi} = 6 \times 10^{-8}, \;\; \Psi_{\mathrm{osc}} = 8 \times 10^{-12}, \qquad M = 5.5 \times 10^{5}\,M_{\odot}.$$

→ High formation redshift: $z \sim 10^5$

Probability of encounter of a neutron star with such a cloud: $P_{\mathrm{enc}} \simeq 0.003$

Probability of capture (loss of energy by dynamical friction): $P_{\mathrm{cap}} \simeq 4 \times 10^{-8}$

→
- increase the star formation rate in such ULDM clouds ?
- observe 2 BH/pulsar binary systems (DM spike generated by the BH)